Journal of Biomedical Nanotechnology
Vol. 4, 359–366, 2008

Role of Lipids in Enhancing Splenic Uptake of Polymer-Lipid (LIPOMER) Nanoparticles

Rajesh R. Patil[1], Rajiv V. Gaikwad[2], Abdul Samad[2], and Padma V. Devarajan[1,*]

[1] *Department of Pharmaceutical Sciences and Technology, University Institute of Chemical Technology, University of Mumbai, Mumbai 400019, India*
[2] *Veterinary Nuclear Medicine Center, Department of Medicine, Bombay Veterinary College, Parel, Mumbai 400012, India*

A number of intracellular infections are primarily resident in the spleen. The aim of present study was to evaluate the splenotropic potential of lipids reported in the preparation of solid lipid nanoparticles. A nanoparticulate system comprising of a hydrophilic polymer-lipid (LIPOMER) combination was selected. Nanoparticles of doxycycline hydrochloride, a highly water soluble drug and drug of choice for intracellular infections, were prepared by nanoprecipitation. Nanoparticles exhibited high drug entrapment efficiency and nanosize. Location of lipid in the nanoparticles was evaluated by transmission electron microscopy. Comparative biodistribution studies in rats, using ^{99m}Tc labeled formulations revealed enhanced splenic uptake of nanoparticles containing glyceryl monostearate as lipid. Further, the organ associated radioactivity of liver and spleen suggested significant enhancement in splenic uptake at concentrations of glyceryl monostearate ($\geq$25%). Our findings suggest the splenotropic potential of glyceryl monostearate which could have ramifications for delivery of a number of agents to the spleen.

Keywords: Lipids, Polymeric Nanoparticles, Doxycycline Hydrochloride, Scintigraphy, Glyceryl Monostearate, Splenic Uptake.

RESEARCH ARTICLE

1. INTRODUCTION

Intracellular infections like syphilis, kala azar, infectious mononucleosis, psittacosis are predominantly localized in the spleen. Further, infections in animals like ehrlichiosis,[1] trypanosoma,[2] brucellosis,[3] and turkey herpes virus[4] are also primarily resident in the spleen with infections like ehlriochiosis, and brucellosis[3,5] known to be zoonotic. Literature abounds in reports of generalized targeting to the RES using colloidal drug carriers such as liposomes,[5–8] niosomes,[9] microparticles,[10–12] polymeric nanoparticles,[7,13–16] and nanosuspensions[17] however concerted efforts in the design of splenotropic drug delivery systems which could provide significant advantage in the treatment of such infections are limited.

The spleen receives barely 15% of an injected dose of colloidal drug delivery system due to phagocytosis by the Kupffer cells.[18] A concise review by Moghimi discusses the various approaches to bypass hepatic uptake thereby enhancing splenic drug concentration.[19] Increased splenic uptake has been associated with large particle size carriers.[20] However alteration of surface properties permitted splenic entrapment of smaller particles following intravenous injection. Coating of small particles (150–250 nm) with block co-polymer surfactants poloxamer 407 and poloxamine 908 enhanced splenic uptake in rats.[21,22] This enhancement was species dependent and not observed in mice and rabbits.[23,24] Higher spleen accumulation of PEGylated polylactic acid and poly(methoxypolyethyleneglycol cyano acrylate-co-hexadecyl cyanoacrylate) nanoparticles has been reported.[25,26] Fattal et al. have reported marked reduction in splenic bacterial counts with liposomal ampicillin compared to ampicillin loaded polybutylisohexylcyanoacrylate nanoparticles in the treatment of Listeria infections in mice.[8,13,27]

The effect of lipid on splenotropic behaviour of liposomes has been reported. Ganglioside GM1 and PEG-5000 phosphatidyl ethanolamine containing liposomes are reported to bypass Kupffer cell uptake in mice.[28,29] Liposomes of size less than 200 nm containing cholesterol as lipid, readily bypassed Kupffer cells and exhibited higher splenic uptake which was dependent on the cholesterol concentration.[30] The above reports which suggest the splenotropic potential of lipids are limited to the lipids used in liposomal formulations.

Liposomal systems pose several constraints, such as physical instability, chemical instability of the phospholipids and drug leakage.[31] Nanoparticles however exhibit

*Author to whom correspondence should be addressed.

 1550-7033/2008/4/359/008 doi:10.1166/jbn.2008.320

greater stability and higher drug entrapment compared to liposomes. The RES uptake of solid lipid nanoparticles (SLN) is well reported,[32, 33] nevertheless their splenotropic behavior is unexplored. The present study is an attempt to screen lipids used in SLN for enhanced splenic uptake. Doxycycline hydrochloride (DH) is a water soluble drug (Log P: −0.2, pKa: 3.1) and drug of choice for bacterial and protozoal intracellular infections predominant in the spleen. As SLN is known to exhibit poor entrapment efficiency of hydrophilic drugs,[34, 35] a nanoparticulate system of DH comprising of a hydrophilic polymer-lipid combination (LIPOMER)[36] was selected in present study. We postulated that this combination would permit high drug entrapment efficiency due to the hydrophilic polymer.

2. MATERIAL AND METHODS

2.1. Materials

Doxycycline hydrochloride was a gift sample from M/s Alembic, India. Gantrez AN 119 [poly(methylvinylether-co-maleic anhydride)] (ISP) was gifted by Anshul Agencies India. Geleol (Glyceryl monostearate), Plurol Stearique (Polyglyceryl distearate), Precerol ATO (Glyceryl palmitostearate) of Gatefosse were gifted by Colorcon Asia and Dynasan 118 (Glyceryl tristearate) of Sasol, was a gift sample from S. Zhaveri Pharmakem, India. Lubritab (hydrogenated vegetable oil) was a gift sample from Penwest, USA. Stearic acid and Docusate sodium were purchased from SD Fine Chem., India. ^{99}Molybdenum was procured from Board of Radiation and Isotope Technology (BRIT) (Mumbai, India). Sodium pertechnetate (^{99m}Tc) was extracted from ^{99}Molybdenum by solvent extraction. All other chemicals and solvents were either spectroscopic or analytical grade. Water was obtained by double distillation from glass stills.

2.2. Preparation of DH LIPOMER (LNP)

DH LNP were prepared by nanoprecipitation technique using poly(methylvinylether-co-maleic anhydride) and lipid as matrix material. Briefly, poly(methylvinylether-co-maleic anhydride) (200 mg), DH (100 mg), and the lipid (100 mg) were dissolved in a mixture of 5 ml tetrahydrofuran (THF) and 2 ml isopropyl alcohol. An aqueous solution of docusate sodium (100 mg) was prepared in 30 ml mixture of water: isopropyl alcohol (1:1). Organic phase was added to the aqueous phase with magnetic stirring. Crosslinking of the polymer matrix was achieved by addition of 3 ml of 5% w/v aqueous solution of magnesium acetate. The dispersion was stirred for 4 hrs to allow complete evaporation of organic solvent. Nanoparticles were separated by centrifugation at 15,000 RPM for 30 min. The resultant pellet was dispersed in 5 ml distilled water using a probe sonicator (Vibronics ultrasonic processor P2, India, 20 KHz) for 5 min. The dispersions were lyophilized after addition of 40 mg fructose as cryoprotectant. The lipids evaluated included glyceryl monostearate (DH LNP 1), glyceryl tristearate (DH LNP 2), polyglyceryl distearate (DH LNP 3), glyceryl palmitostearate (DH LNP 4), hydrogenated vegetable oil (DH LNP 5), and stearic acid (DH LNP 6). Batches with varying amounts of lipid (glyceryl monostearate) were prepared by changing polymer: lipid proportion, DH LNP 1(0.5) containing poly(methylvinylether-co-maleic anhydride) (250 mg), DH (100 mg) and glyceryl monostearate (50 mg) while DH LNP 1(1.5) containing poly(methylvinylether-co-maleic anhydride) (150 mg), DH (100 mg), glyceryl monostearate (150 mg).

DH LNP 1W was prepared by modifying the aqueous phase of DH LNP 1, wherein the hydroalcoholic phase [water: isopropyl alcohol (1:1)] was replaced with water as the aqueous phase (DH LNP 1W). DH polymeric nanoparticles (DH NP) and DH solid lipid nanoparticles (DH SLN) were prepared following the same method omitting lipid/polymer respectively.

2.3. Entrapment Efficiency

Entrapment efficiency was determined by analysis of the supernatant for free drug after centrifugation (15,000 RPM for 30 min) of the nanoparticulate dispersion during the preparation of nanoparticles. Supernatant was diluted 100 times with water and analyzed by UV spectrophotomety (Shimadzu, Japan) at λmax 275 nm. The % entrapment efficiency was calculated using Eq. (1),

$$\%\ \text{Entrapment efficiency} = ([\text{DH}]_{\text{total}} - [\text{DH}]_{\text{supernatant}})/[\text{DH}]_{\text{total}} \times 100 \quad (1)$$

2.4. Particle Size Determination

The particle size was measured by Photon Correlation Spectroscopy using Coulter N4 plus submicron particle size analyzer (Beckman Coulter) by scattering light at 90° at 25 °C. The nanoparticulate dispersion was diluted appropriately with water, filtered through 0.45 μm, to obtain final counts per second (Intensity), 5×10^4 to 1×10^6.

2.5. Transmission Electron Microscopy (TEM)

Copper grids (Cu 200, EM Sciences) were immersed in dispersions of DH NP, DH LNP 1 and DH LNP 1W and left undisturbed overnight at 4 °C to allow their deposition on the grid. The grids were then washed thrice with distilled water. Freshly prepared aqueous phosphotungstanic acid solution (10 mg ml^{-1}) was used as negative staining agent. Grids were treated with phosphotungstanic acid solution for 30 seconds and washed five times with distilled water. Stained samples were finally vacuum dried.

The TEM images of stained DH NP, DH LNP 1 and DH LNP 1W were recorded on Techni G^2 TEM (FEI, Eindohoven, Netherlands).

2.6. Differential Scanning Calorimetry (DSC)

Thermal behavior of the formulations was determined by differential Scanning Calorimetry. Powdered samples were accurately weighed (5 mg) in aluminum pans, sealed and subjected to differential scanning calorimetry under nitrogen flow using a Perkin Elmer Pyris 6 DSC thermal analysis instrument. Thermograms were recorded by heating samples from 35 °C to 400 °C at a heating rate of 10 °C min^{-1} with empty aluminum pan as the reference.

2.7. Fourier Transform Infrared Spectroscopy (FTIR) Studies

FTIR studies were performed on Perkin Elmer RX1 using a KBr pellet to check drug excipient interaction. Briefly, each sample was crushed to a fine powder, mulled with KBr and compressed to form a thin transparent pellet and IR spectroscopy was performed.

2.8. Radiolabelling of DH, DH NP and DH LNP

DH, DH NP and DH LNP were labeled with ^{99m}Tc after reduction with stannous chloride. Briefly, 150 μl stannous chloride solution in 0.1 N HCl (10 mg ml^{-1}) was added to ^{99m}Tc (1.5 mCi) in normal saline. This was followed by immediate addition of 1.5 ml of DH solution, DH nanoparticles or DH LNP dispersion equivalent to 10 mg ml^{-1} DH and 1 ml of pH 6.8 Tris buffer. The mixture was then agitated for 20 min on a shaker at 28 °C.

Radiolabelling efficiency was determined by minor modification of a reported method.[37] The radiolabelled formulation was spotted on a High performance thin layer chromatography (HPTLC) plate at a distance of one cm from the lower end and developed using acetone as the mobile phase. Solvent was allowed to travel 10 cm from the origin. The plate was removed, dried, and cut in two equal halves. The radioactivity in each half was determined under Millennium MPS Acquisition System, (Multipurpose Single Head Square Detector) Gamma Camera fitted with Low Energy General Purpose (LEGP) collimator manufactured by G.E. (General Electric). The data acquisition from the gamma camera was performed with a computer 'Acquisition System.' The data was acquired on GENIE acquisition station and then transferred to eNTEGRA workstation for processing. The processing software was part of the gamma camera system. Static images were acquired and stored digitally in a 256 × 256 matrix. Radioactivity in each part was determined as counts per minute (cpm) in the region of interest. Radioactivity corresponding to the lower half was regarded as (formulation) bound activity while the radioactivity corresponding to the upper half was regarded as unbound (free) activity (R_f of ^{99m}Tc = 0.9). The percent radiolabelling efficiency was represented as percent ratio of bound activity to total activity. Stability of radiolabelled complex was determined by monitoring radiolabelling efficiency upto 6 hr at 28 °C.

Formation of radiocolloids is undesirable while radiolabelling since it may give misleading results *in vivo*.[38] Radiocolloid formation was determined by chromatographic technique using pyridine: acetic acid: water (3:5:1.5) as the separation system by minor modification of a reported method.[37] The radiolabelled formulation was spotted on a HPTLC plate at a distance of one cm from lower end and developed using the mobile phase. Solvent was allowed to travel 10 cm from the origin. The plate was removed, dried, and cut in two equal halves. The radioactivity in each half was determined under gamma camera (GE) by determining counts per minute (cpm) in the region of interest. Radiocolloids were retained at the bottom ($R_f = 0$) while free pertechnetate and labeled complex migrated with solvent front.

2.9. Biodistribution Studies

Biodistribution studies were carried out in wistar rats of either sex, 6–8 weeks old, weighing 200–250 g ($n = 4$). Rats were housed under standard conditions and had free access to water and were fed standard laboratory chow. All experiments were approved by the Animal Welfare Committee of institute. Animals were anesthetized by injecting a ketamine hydrochloride (50 mg kg^{-1}) and xylazine hydrochloride (10 mg kg^{-1}) cocktail intramuscularly 20 min prior to study.

The animals were placed prone on a Millennium MPS Acquisition System, (Multipurpose Single Head Square Detector) Gamma Camera fitted with Low Energy General Purpose (LEGP) collimator. The distance of collimator to table was maintained at 95 cm for all acquisitions. Doxycycline hydrochloride (10 mg kg^{-1}) as radiolabelled DH, DH nanoparticles and DH LNP (approx. 500 μCi) was injected intravenously into the tail vein. For the purpose of determining total injected dose the radioactivity of syringe before and after dosing in form of static images was acquired for one minute. Regions of interest were drawn in the static image and radioactivity in the same was accessed as described in radiolabelling of DH. Total injected dose was estimated by subtracting radioactivity after dosing from radioactivity before dosing. At each hour, up to five hours post dosing, static images were recorded for a period of 5 min each at 1.33× zoom. All the static images were stored digitally in a 256 × 256 matrix.

At the end of five hours animals were sacrificed, and heart, spleen, lungs, stomach, liver, and small intestine were isolated. The organs were washed three times with saline, blot dried and weighed. The radioactivity counts per minute (cpm) in each organ was determined under

gamma camera by drawing region of interest and corrected for physical decay. The % injected dose g^{-1} of organ was calculated and normalized to % using the Eq. (2)

$$\%\ \text{injected dose}_{\text{organ}} = \frac{\%\ \text{injected dose}\ g^{-1}_{\text{organ}}}{\text{Total}\ \%\ \text{injected dose in organs}} \times 100 \quad (2)$$

3. DATA ANALYSIS

All data in tables and the figures are expressed as mean ± standard deviation and mean ± standard error respectively. Statistical analysis was performed using the one-way ANOVA with Tukey-Kramer HSD and Student's *t* tests. $P < 0.05$ was the criterion for statistical significance.

4. RESULTS AND DISCUSSION

4.1. Entrapment Efficiency and Particle Size

Figure 1(a) depicts effect of nanoparticles matrix material on entrapment efficiency. DH nanoparticles made from hydrophilic polymeric matrix revealed high entrapment efficiency (91%) while DH SLN made from hydrophobic lipid matrix revealed poor entrapment efficiency (15%) ($p < 0.001$). The hydrophobic matrix of SLN poses unfavorable environment for hydrophilic DH, forcing it to partition into the aqueous phase during the manufacturing process. Low entrapment efficiency of DH in SLN would mean high amount of carrier required to administer therapeutic dose of drug and moreover tremendous wastage of drug during manufacture.

Entrapment efficiency of DH LNP 1–6 was also higher than SLN ($p < 0.001$) and dependent on type of lipid (Fig. 1(a)). High entrapment efficiency observed in LNP may be explained by the presence of hydrophilic polymeric matrix which prevented lipid mediated expulsion of hydrophilic drug. Entrapment efficiency was seen to be in the order DH LNP 1 > DH LNP 2 = DH LNP 3 > DH LNP 6 > DH LNP 4 > DH LNP 5 > DH LNP 1W. Maximum entrapment efficiency of DH LNP 1 comparable to DH NP ($p > 0.05$) could be due to minimum hydrophobicity of glyceryl monostearate compared to other lipids evaluated in this study. Replacing isopropyl alcohol with water revealed poor entrapment efficiency (DH LNP 1W) due to loss of drug in the aqueous phase.

While no significant difference in entrapment efficiency was observed with DH LNP 1(0.5) and DH LNP 1 ($p > 0.05$), entrapment efficiency decreased significantly ($p < 0.001$) with further increase in lipid concentration [DH LNP 1(1.5)] (Fig. 2).

DH LNP exhibited higher particle size compared to DH nanoparticles except for DH LNP 3 (Fig. 1(b)), which exhibited a lower size ($p < 0.001$). Further, increase in lipid concentration also revealed increase in particle size (Fig. 2). Increase in particle size could be correlated

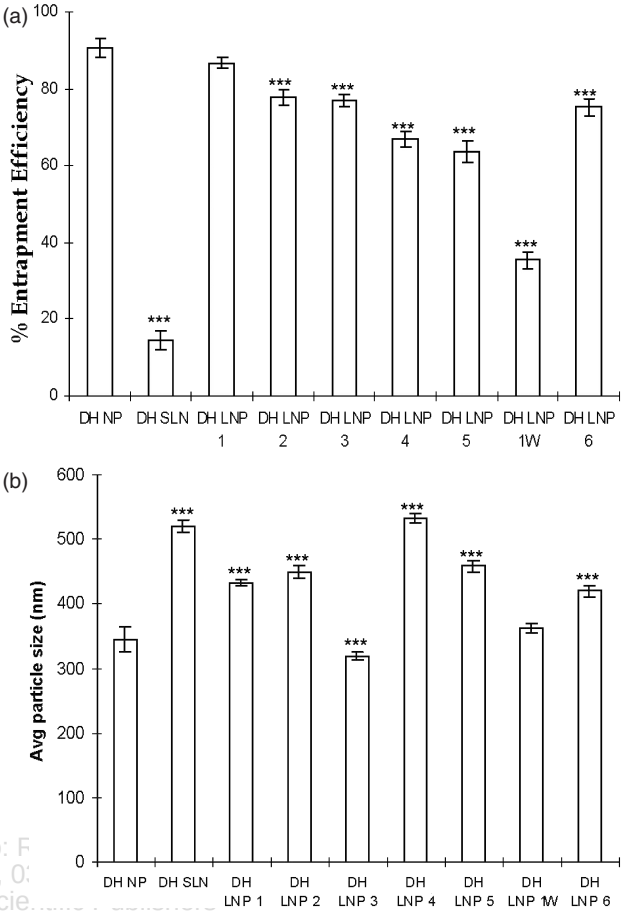

Fig. 1. Effect of nanoparticles matrix material on (a) % entrapment efficiency and (b) average particle size (nm) of DH nanoparticle formulations (mean ± standard error, ($n = 4$), $^{***}p < 0.001$ between DH NP and other formulations).

to increased viscosity of organic phase due to the lipids. More viscous organic phase provides higher mass transfer resistance thus resulting in formation of larger nanoparticles.[39]

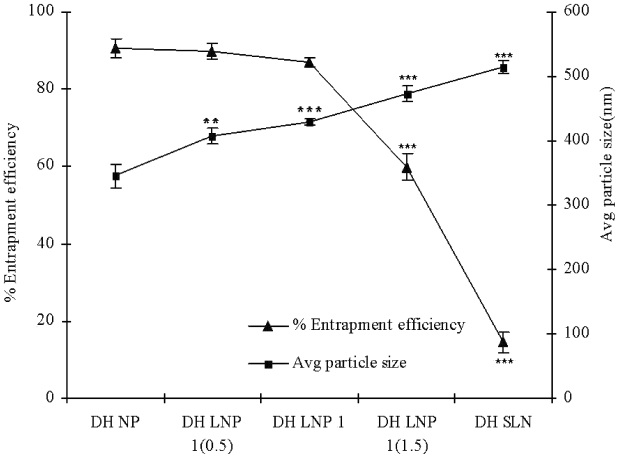

Fig. 2. Effect of glyceryl monostearate concentration on % entrapment efficiency and average particle size (nm) (mean ± standard error, ($n = 4$), $^{***}p < 0.001$, $^{**}p < 0.01$ between DH NP and other formulations).

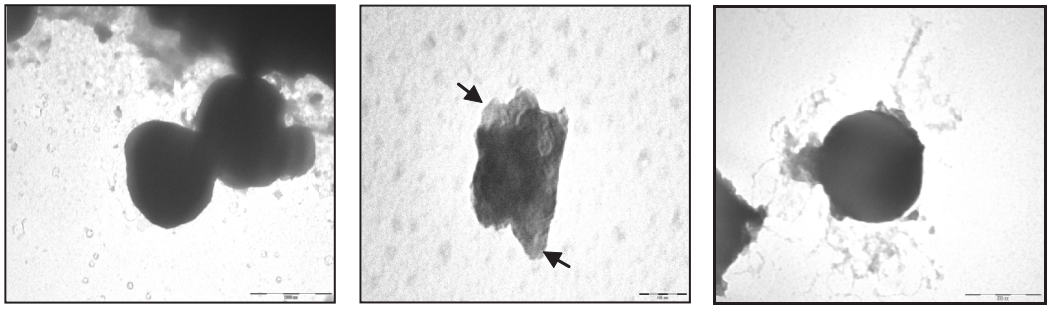

Fig. 3. Transmission electron micrographs of DH nanoparticle formulations, (a) DH NP, (b) DH LNP 1, (c) DH LNP 1W. (Scale bar 200 nm) (→) Indicates presence of surface anchored lipid.

4.2. Transmission Electron Microscopy (TEM)

Transmission electron micrographs of negatively stained samples of DH nanoparticles and DH LNP 1W appeared similar and homogenous while TEM images of DH LNP 1 revealed surface anchoring of lipid (Figs. 3(a–c).). Addition of organic phase containing polymer, lipid and drug into aqueous phase containing stabilizer creates a concentration gradient, surface tension variation at the interface inducing interfacial turbulence dictated by Marangoni or the ouzo effect.[40–42] Bidirectional diffusion between organic solvents and water at the concentration gradients results in local region of supersaturation leading to nano-structured precipitation of polymer entrapping the drug.[43] This bidirectional diffusion favored movement of lipid towards the surface of nanoparticles when the aqueous phase contained isopropyl alcohol, a good solvent for the lipid. Use of isopropyl alcohol in the aqueous phase therefore enabled surface anchoring of the lipid (Fig. 3(b)). In contrast, in case of DH LNP 1W prepared with water as aqueous phase the lipid prefers to remain in the LNP core due to non solvent effect of water (Fig. 3(c)). Surface anchoring of lipid could permit better recognition by macrophage for subsequent uptake.

4.3. Differential Scanning Calorimetry (DSC)

DSC thermograms of DH, poly(methylvinylether-co-maleic anhydride), DH NP, DH LNP 1 and glyceryl monostearate are depicted in Figure 4. DSC thermograms revealed no interaction between drug and excipients moreover absence of melting endotherm of DH in case of DH NP and DH LNP 1 suggested that the drug was molecularly dispersed in the nanoparticle matrix. Moreover, XRD spectra confirmed absence of crystalline drug (data not reported).

4.4. Fourier Transform Infrared Spectroscopy (FTIR) Studies

FTIR studies are rapid method of accessing drug: excipient interaction in the formulation. FTIR of DH NP and DH LNP 1 revealed all the characteristic peaks of DH such as band due to O–H/N–H stretching vibrations appearing at 3388 cm^{-1}, while those due to the C–H stretching

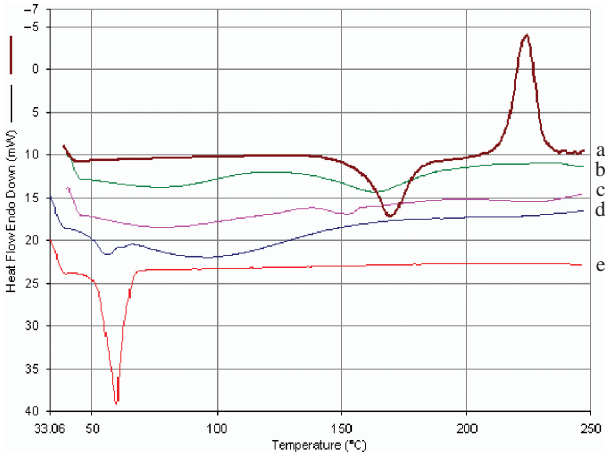

Fig. 4. Comparative DSC thermograms of (a) DH, (b) poly(methylvinylether-co-maleic anhydride), (c) DH NP, (d) DH LNP 1, (e) glyceryl monostearate.

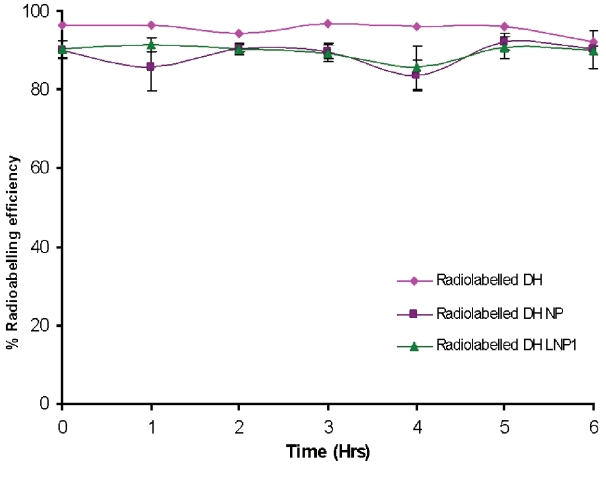

Fig. 5. Radiolabelling stability study of ^{99m}Tc labelled DH, DH NP and DH LNP 1 by chromatographic technique at 28 °C (mean ± standard error, $n = 3$).

RESEARCH ARTICLE

Table I. Comparative biodistribution profile 5 hours post dosing of ^{99m}Tc and ^{99m}Tc labeled DH formulations in Wistar rats represented as % dose in organ.

	% Injected dose							
Organ	^{99m}Tc	DH Solution	DH NP	DH LNP 2	DH LNP 3	DH LNP 4	DH LNP 5	DH LNP 6
Heart	1.89 ± 1.67	1.57 ± 0.54	1.28 ± 1.03	3.67 ± 0.50	2.97 ± 0.89	2.56 ± 1.93	2.16 ± 0.54	4.47 ± 1.17
Lung	4.03 ± 1.60	11.41 ± 4.28	24.30 ± 6.29	16.09 ± 7.01	17.89 ± 7.61	5.64 ± 2.78	21.89 ± 7.44	11.94 ± 5.14
Liver	4.60 ± 1.13***	21.55 ± 1.03***	38.43 ± 6.45	34.92 ± 0.24	45.96 ± 5.32	42.87 ± 4.18	40.17 ± 6.67	35.34 ± 3.88
Spleen	2.27 ± 1.98***	7.85 ± 2.95***	25.48 ± 0.77	33.74 ± 2.81	15.06 ± 3.06***	18.57 ± 0.84***	15.82 ± 1.71***	25.08 ± 1.70
Stomach	74.44 ± 10.98	2.80 ± 1.82	4.09 ± 2.67	2.38 ± 0.38	3.12 ± 2.18	6.33 ± 0.96	2.14 ± 0.30	5.26 ± 0.16
Intestine	12.76 ± 8.21	54.82 ± 4.01	6.42 ± 1.72	9.20 ± 4.74	15.00 ± 2.60	24.03 ± 2.33	17.83 ± 0.72	17.92 ± 1.04

Mean ± standard deviation, ($n = 4$), *** $p < 0.001$ between DH NP and other formulations.

vibrations are observed at 2916 and 2853.5 cm^{-1}. Bands due to primary amide (N–H) bending and aromatic N–H bending vibrations are observed at 1673 and 1581 cm^{-1}, respectively. Carbonyl (C═O) stretching vibrations at 1616 cm^{-1}, and the bands at 1456.6 and 1321.7 cm^{-1} due to $–CH_2$ bending and C–H bending vibrations, respectively. No drug: excipient interaction was evident in the spectra.

4.5. Radiolabelling and *In Vitro* Stability of Radiolabelled Complexes

DH and DH formulations were labeled using reduced ^{99m}Tc for scintigraphic studies. Reduction of ^{99m}Tc and subsequent binding to DH formulations were found to be dependent on $SnCl_2$ concentration and pH of the buffer (data not shown). While lower concentrations of $SnCl_2$ are reported to result in poor labeling efficiency, higher concentrations resulted in formation of radiocolloids. Our radiolabelling studies were optimized at $SnCl_2$ concentration 1 mg mci^{-1}. Good radiolabelling efficiency (85%) with adequate stability was observed (Fig. 5). Further absence of radiocolloid was confirmed using pyridine: acetic acid: water (3:5:1.5) as the separation system.

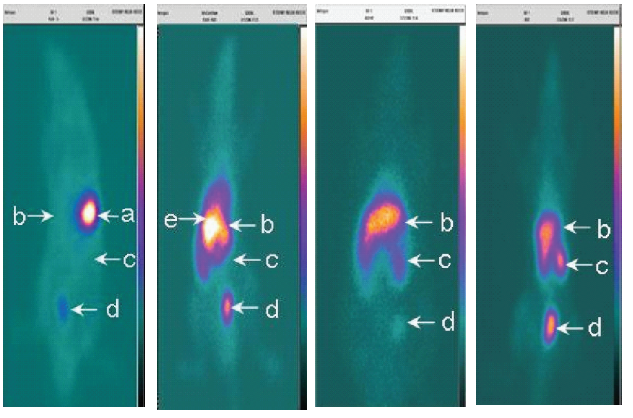

Fig. 6. Gamma scintigraphic images depicting biodistribution profile post 5 hr dosing of (I) ^{99m}Tc, (II) DH solution, (III) DH NP, (IV) DH LNP 1 in Wistar rats. Markers: a – stomach, b – liver, c – spleen, d – bladder, e – intestine.

4.6. Biodistribution Studies of ^{99m}Tc and DH formulations

Comparative biodistribution profiles of radiolabelled DH, radiolabelled DH nanoparticles and ^{99m}Tc are depicted in Table I. DH SLN were not taken up for the study due to poor drug entrapment (Fig. 1). Significant difference in biodistribution profiles of free ^{99m}Tc compared with radiolabelled DH and DH nanoparticles (both NP and LNP), suggested ^{99m}Tc formed a stable ligand with DH formulations *in vivo*. DH is primarily metabolized by the liver and ultimately excreted through the feces. This accounts for the high level of radioactivity in the intestine.

DH NP and DH LNP were seen to localize in the reticuloendothelial system organs (Table I). Maximal radioactivity was seen in the liver with all the formulations except DH LNP 1 comprising glyceryl monostearate as the lipid. Splenic uptake was seen to be significantly higher with DH LNP 1 (Fig. 6). This enhanced splenic uptake was concentration dependent and increased as the concentration of glyceryl monostearate increased (Table II). Further, the organ associated radioactivity (Fig. 7) of liver and spleen suggested a significant enhancement in splenic uptake at concentrations of glyceryl monostearate (≥25%).

The biodistribution data of LNP 1W, despite comprising glyceryl monostearate as lipid, revealed a profile similar to DH NP. This effect is explained by the TEM study. TEM of DH LNP 1W (Fig. 3(c)) suggests the entrapment of glyceryl monostearate in the core of the nanoparticle, in contrast

Table II. Role of glyceryl monostearate on the biodistribution profile of ^{99m}Tc labeled DH LNP formulations represented as % injected dose in organ 5 hours post dosing in Wistar rats.

	% Injected dose			
Organ	DH LNP 1(0.5)	DH LNP 1	DH LNP 1(1.5)	DH LNP 1W
Heart	2.14 ± 1.36	1.83 ± 0.72	1.55 ± 0.98	1.00 ± 0.81
Lung	20.44 ± 5.28	11.65 ± 3.43	9.60 ± 2.12	23.07 ± 1.13
Liver	30.64 ± 2.77	26.27 ± 6.03	25.11 ± 3.73	40.86 ± 1.35***
Spleen	33.13 ± 5.43***	50.16 ± 8.54	58.08 ± 7.01	24.36 ± 3.35***
Stomach	3.27 ± 1.31	1.57 ± 2.04	1.05 ± 0.48	4.87 ± 2.03
Intestine	10.37 ± 8.62	8.52 ± 3.89	4.60 ± 1.08	5.84 ± 0.66

Mean ± standard deviation, ($n = 4$), *** $p < 0.001$ between DH LNP 1 and other formulations.

RESEARCH ARTICLE

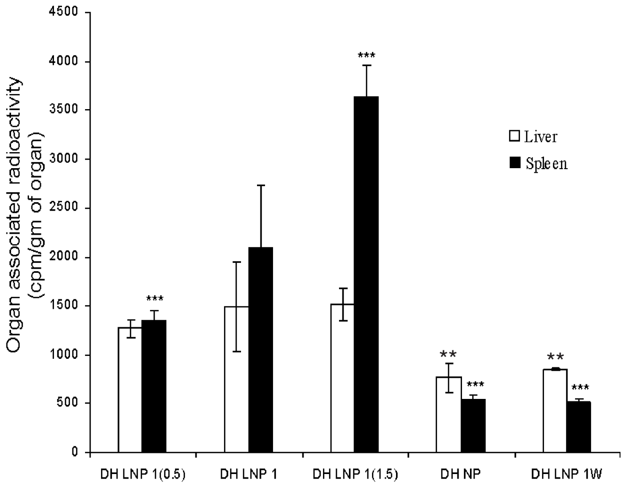

Fig. 7. Effect of glyceryl monostearate on organ associated radioactivity (cpm g^{-1}) 5 hours after IV injection of radiolabelled DH polymer nanoparticle formulations in Wistar rats (mean ± standard error, ($n = 4$), $^{***}p < 0.001$ and $^{**}p < 0.01$ between DH LNP 1 and other formulations).

to surface anchored glyceryl monostearate in DH LNP 1 (Fig. 3(b)). Enhanced splenic uptake with DH LNP 1 and DH LNP 1(1.5) and no change in splenic uptake observed with DH LNP 1W substantiates the splenotropic behavior of glyceryl monostearate. This finding could have ramifications for delivery of a number of agents to the spleen.

Plant glycosides are reported as macrophage targeting agents.[44] It has been suggested that the hydrophobic part (aglycone) is usually buried in the carrier matrix and the hydrophilic glycosidic chain facing aqueous medium acts as ligand for the carbohydrate recognizing receptor (such as mannosyl fucosyl receptor) located on macrophages.[9,45] This conformation is akin to lipopolysaccharides generally present on the cell walls of many species of bacteria which are able to interact with family of mannosyl fucosyl receptors on macrophage and evoke immune response.[46]

Glyceryl monostearate due to presence of a hydrophobic part (stearic acid) and hydrophilic part (glycerol) probably mimics the glycosides by presenting an optimum conformation to bind efficiently to mannosyl fucosyl receptor located on the macrophage surface. Further DH LIPOMERs with stearic acid (DH LNP 6) as the lipid did not reveal splenotropic behaviour. This hypothesis is being confirmed by receptor docking and macrophage cell uptake studies.

5. CONCLUSION

We report the splenotropic potential of a stable and biodegradable lipid glyceryl monostearate. LIPOMERs of DH containing glyceryl monostearate present an improved strategy for the delivery of hydrophilic drugs for the treatment of infections predominant in the spleen. Evaluation in clinical models of infection would be taken up to confirm the same.

Acknowledgments: The authors thank Director, National Institute of Reproductive Research and Health (NIRRH), Mumbai and Dr. Geeta Vanage, Deputy Director, NIRRH, for TEM studies.

References and Notes

1. S. Harrus, T. Waner, A. Keysary, I. Aroch, H. Voet, and H. Bark, Investigation of splenic functions in canine monocytic ehrlichiosis. *Vet. Immunol. Immunopathol.* 62, 15 **(1998)**.
2. R. C. Melo and Z. Brener, Tissue tropism of different Trypanosoma cruzi strains. *J. Parasitol.* 64, 475 **(1978)**.
3. M. Doganay and B. Aygen, Human brucellosis: An overview. *Int. J. Infect. Dis.* 7, 173 **(2003)**.
4. J. Fabricant, B. W. Calnek, and K. A. Schat, The early pathogenesis of Turkey Herpes virus infection in Chickens and Turkeys. *Avian Dis.* 26, 257 **(1982)**.
5. C. R. Alving, Macrophages as targets for delivery of liposome encapsulated antimicrobioal agents. *Adv. Drug Deliv. Rev.* 2, 107 **(1988)**.
6. P. F. Bonventre and G. Gregoriadis, Killing of intraphagocytic *Staphylococcus aureus* by dihydrostreptomycin entrapped within liposomes. *Antimicrob. Agents Chemother.* 13, 1049 **(1978)**.
7. J. Kreuter, Liposomes and nanoparticles as vehicles for antibiotics. *Infection* 19, S224 **(1991)**.
8. E. Fattal, J. Rojas, M. Youssef, P. Couvreur, and A. Andremont, Liposome-entrapped ampicillin in the treatment of experimental murine listeriosis and salmonellosis, *Antimicrob. Agents Chemother.* 35, 770 **(1991)**.
9. S. Medda, S. Mukhopadhyay, and M. K. Basu, Evaluation of the *in-vivo* activity and toxicity of amarogentin, an antileishmanial agent, in both liposomal and niosomal forms. *J. Antimicrob. Chemother.* 44, 791 **(1999)**.
10. A. J. Baillie Coombs, G. H. Dolan, T. F. Hunter, T. Laakso, I. Sjoholm, and P. Stjarnkvist, Biodegradable microspheres: Polyacryl starch microparticles as delivery system for the antileishmanial drug, sodium stibogluconate. *J. Pharm. Pharmacol.* 39, 832 **(1987)**.
11. S. Medda, P. Jaisankar, R. K. Manna, B. Pal, V. S. Giri, and M. K. Basu, Phospholipid microspheres: A novel delivery mode for targeting antileishmanial agent in experimental leishmaniasis. *J. Drug Target.* 11, 123 **(2003)**.
12. Y. Tabata and Y. Ikada, Effect of the size and surface charge of polymer microspheres on their phagocytosis by macrophage. *Biomaterials* 9, 356 **(1988)**.
13. M. Youssef, E. Fattal, M. Alonso, L. Roblot-Treupel, J. Sauzieres, C. Tancrede, A. Omnts, P. Couvreur, and A. Andremont, Effectiveness of nanoparticle-bound ampicillin in the treatment of Listeria monocytogenes infection in athymic nude mice. *J. Antimicrob. Chemother.* 32, 1204 **(1988)**.
14. F. Forestier, P. Gerrier, C. Chaumard, A. M. Quero, P. Couvreur, and C. Labarre, Effect of nanoparticle bound ampicillin on the survival of *Listeria monocytogenes* in mouse peritoneal macrophages. *J. Antimicrob. Chemother.* 30, 173 **(1992)**.
15. Q. Zhang, G. Liao, D. Wei, and T. Nagai, Increase in gentamicin uptake by cultured mouse peritoneal macrophages and rat hepatocytes by its binding to polybutylcyanoacrylate nanoparticles. *Int. J. Pharm.* 164, 21 **(1998)**.
16. C. Lecaroz, C. Gamazo, and M. J. Blanko-Pirto, Nanocarriers with gentamycin to treat intracelluar pathogens. *J. Nanosci. Nanotechnol.* 6, 3296 **(2006)**.
17. N. Scholer, K. Krause, O. Kayser, R. H. Müller, K. Borner, H. Hahn, and O. Liesenfeld, Atovaquone nanosuspensions show excellent therapeutic effect in a new murine model of reactivated toxoplasmosis. *Antimicrob. Agents Chemother.* 45, 1771 **(2001)**.

18. I. A. Bakker-Woudenberg, A. F. Lokerse, J. C. Vink-van der Berg, and F. H. Roerdink, Liposome encapsulated ampiiIlin against Listeria monocytogenes *in vivo* and *in vitro*. *Infection* 16, S165 **(1988)**.

19. S. M. Moghimi, Mechanisms of splenic clearance of blood cells and particles: Towards development of new splenotropic agents. *Adv. Drug Deliv. Rev.* 17, 103 **(1995)**.

20. C. Li, D. J. Yang, L. R. Kuang, and S. Wallace, Polyamino acid microspheres: Preparation, characterization and distribution after intravenous injection in rats. *Int. J. Pharm.* 94, 143 **(1993)**.

21. S. M. Moghimi, C. J. H. Porter, I. Muir, L. Illum, and S. S. Davis, Non-phagocytic uptake of intravenously injected microspheres in rat spleen: Influence of particle size and hydrophilic coating. *Biochem. Biophys. Res. Commun.* 177, 861 **(1991)**.

22. S. M. Moghimi, H. Hedeman, I. S. Muir, L. Illum, and S. S. Davis, An investigation of the filtration and the fate of large filtered sterically-stabilized microspheres in rat spleen. *Biochim. Biophys. Acta* 1157, 233 **(1993)**.

23. L. Illum, S. S. Davis, R. H. Müller, E. Mak, and P. West, The organ distribution and circulation time of intravenously injected colloidal carriers sterically stabilized with a block copolymer–poloxamine 908. *Life Sci.* 40, 367 **(1987)**.

24. S. M. Moghimi, Poloxamer 188 revisited: A potentially valuable immunomodulator. *J. Nat. Cancer Inst.* 88, 766 **(1996)**.

25. D. Bazile, C. Prud'homme, M. T. Bassoullet, M. Marlard, G. Spenlehauer, and M. Veillard, Stealth MePEG-PLA nanoparticles avoid uptake by the mononuclear phagocyte system. *J. Pharm. Sci.* 84, 493 **(1995)**.

26. M. T. Peracchia, E. Fattal, D. Desmaele, M. Besnard, J. P. Noel, J. M. Gomis, M. Appel, J. d'Angelo, and P. Couvreur, Stealth PEGylated polycyanoacrylate nanoparticles for intravenous administration and splenic targeting. *J. Control. Rel.* 60, 121 **(1999)**.

27. P. Couvereur, E. Fattal, and A. Andremont, Liposomes and nanoparticles in the treatment of intracellular bacterial infections. *Pharm. Res.* 8, 1079 **(1991)**.

28. A. L. Klibanov, K. Maruyama, A. M. Beckerleg, V. P. Torchilin, and L. Huang, Activity of amphipathic poly(ethylene glycol) to prolong the circulation time of liposomes depends on the liposome size and is unfavorable for immunoliposome binding to target. *Biochim. Biophys. Acta* 1062, 142 **(1991)**.

29. D. Liu, A. Mori, and L. Huang, Large liposomes containing ganglioside GM1 accumulate effectively in spleen. *Biochim. Biophys. Acta* 1066, 159 **(1991)**.

30. S. M. Moghimi and H. M. Patel, Tissue specific opsonins for phagocytic cells and their different affinity for cholesterol-rich liposomes. *FEBS Lett.* 233, 143 **(1988)**.

31. G. Storm and J. A. D. Crommelin, Liposomes: quo vadis? *PSTT* 1, 19 **(1998)**.

32. C. Bocca, O. Caputo, R. Cavalli, L. Gabriel, A. Miglietta, and M. R. Gasco, Phagocytic uptake of fluorescent stealth and non-stealth solid lipid nanoparticles. *Int. J. Pharm.* 175, 185 **(1998)**.

33. S. Yang, L. Lu, Y. Cai, J. Zhu, B. Liang, and C. Yang, Body distribution in mice of intravenously injected camptothecin solid lipid nanoparticles and targeting effect on brain. *J. Control. Rel.* 59, 299 **(1999)**.

34. A. J. Almeida, S. Runge, and R. H. Müller, Peptide-loaded solid lipid nanoparticles (SLN): Influence of production parameters. *Int. J. Pharm.* 149, 255 **(1997)**.

35. W. Mehnert and K. Mäder, Solid lipid nanoparticles: Production, characterization and applications. *Adv. Drug Deliv. Rev.* 47, 165 **(2001)**.

36. P. V. Devarajan, A. Samad, R. R. Patil, S. A. Guhagarkar, and R. V. Gaikawad, Functional Carriers for Bioactive Agents, Indian Patent Application 1633/MUM/2006 **(2006)**.

37. L. H. Reddy, R. K. Sharma, K. Chuttani, A. K. Mishra, and R. R. Murthy, Etoposide-incorporated tripalmitin nanoparticles with different surface charge: Formulation, characterization, radiolabeling, and biodistribution studies. *The AAPS Journal* 6, Article 23 **(2004)**.

38. T. Banerjeeb, A. K. Singh, R. K. Sharma, and A. N. Maitra, Labeling efficiency and biodistribution of Technetium-99m labeled nanoparticles: Interference by colloidal tin oxide particles. *Int. J. Pharm.* 289, 189 **(2005)**.

39. M. Cachile, A. M. Cazabat, S. Bardon, M. P. Valignat, and F. Vandenbrouck, Spontaneous spreading of surfactant solutions on hydrophilic surfaces. *Colloids Surf. A: Physicochem. Eng. Aspects* 159, 47 **(1999)**.

40. H. Murakami, M. Kobayashi, H. Takeuchi, and Y. Kawashima, Preparation of poly(lactide-co-glycolide) nanoparticles by modified spontaneous emulsification solvent diffusion method. *Int. J. Pharm.* 187, 143 **(1999)**.

41. F. Ganachaud and J. L. Katz, Nanoparticles and nanocapsules created using the Ouzo effect: Spontaneous emulsification as an alternative to ultrasonic and high-shear devices. *Chem. Phys. Chem.* 6, 209 **(2005)**.

42. D. Quintanar-Guerrero, E. All'emann, H. Fessi, and E. Doelker, Preparation techniques and mechanisms of formation of biodegradable nanoparticles from preformed polymers. *Drug Dev. Ind. Pharm.* 24, 1113 **(1998)**.

43. O. Thioune, H. Fessi, J. P. Devissaguet, and F. Puisieux, Preparation of pseudolatex by nanoprecipitation: Influence of the solvent nature on intrinsic viscosity and interaction constant. *Int. J. Pharm.* 146, 233 **(1997)**.

44. M. K. Basu and S. Lala, Macrophage specific drug delivery in experimental leishmaniasis. *Curr. Mol. Med.* 4, 681 **(2004)**.

45. S. Medda, S. Mukherjee, N. Das, K. Naskar, S. B. Mahato, and M. K Basu, Sugar-coated liposomes: A novel delivery system for increased drug efficacy and reduced drug toxicity. *Biotechnol. Appl. Biochem.* 17, 37 **(1993)**.

46. B. P. Singh, R. S. Chauhan, L. K. Singhal, Toll-like receptors and their role in innate immunity. *Curr. Sci.* 85, 1156 **(2003)**.

Received: 3 March 2008. Revised/Accepted: 19 March 2008.

COMMUNICATION

Particle Shape: A New Design Parameter for Passive Targeting In Splenotropic Drug Delivery

PADMA V. DEVARAJAN,[1] ANIL B. JINDAL,[1] RAJESH R. PATIL,[1] FERNAZ MULLA,[2] RAJIV V. GAIKWAD,[2] ABDUL SAMAD[2]

[1]Department of Pharmaceutical Sciences and Technology, Institute of Chemical Technology, N.P. Marg, Matunga (E), Mumbai 400019, Maharashtra, India

[2]Department of Medicine, Veterinary Nuclear Medicine Center, Bombay Veterinary College, Mumbai 400012, Maharashtra, India

Received 26 June 2009; revised 13 October 2009; accepted 17 November 2009

Published online 20 January 2010 in Wiley InterScience (www.interscience.wiley.com). DOI 10.1002/jps.22052

ABSTRACT: The role of particle size and surface modification on biodistribution of nanocarriers is widely reported. We report for the first time the role of nanoparticle shape on biodistribution. Our study demonstrates that irregular shaped polymer lipid nanoparticles (LIPOMER) evade kupffer cells and localize in the spleen. We also demonstrate the macrophage-evading characteristic of the irregular-shaped LIPOMER. Our results suggest particle shape as an important tool for passive targeting of nanocarriers in splenotropic drug delivery. © 2010 Wiley-Liss, Inc. and the American Pharmacists Association J Pharm Sci 99:2576–2581, 2010

Keywords: drug targeting; lipids; nanoparticles; particle size; scintigraphy

The effect of particle size on biodistribution of nanocarriers is well established. Following intravenous administration, small particles (<30 nm) are eliminated by renal excretion,[1] whereas particles of 30–150 nm are localized in the bone marrow,[2] the heart, the kidney, and the stomach.[3] Larger particles (>200 nm) are rapidly taken up by the mononuclear phagocytic system (MPS) cells and targeted to the reticular endothelial system (RES) mainly the liver.[4] The ideal way out to make nanocarriers invisible to the RES is to make them behave like water.[5,6] Coating with hydrophilic polymers like polyethyleneglycol, polyethyleneoxide, poloxamine, and others masquerade the nanocarriers as water bodies, wherein such stealth carriers offer possibilities to evade the RES.[7] Stealth polymeric nanoparticles >200 nm, however, accumulated in the spleen.[8–10]

The impact of particle size and surface modification on *in vivo* behavior of nanocarriers has been actively investigated. However, there are limited studies on the role of particle shape on biodistribution. It is only recently that the role of particle shape on biodistribution has been suggested.[11,12] While, this has triggered efforts in the design of nanocarriers of nonspherical geometry, no *in vivo* studies are apparent. The present article focuses on particle shape as a novel passive targeting approach in the design of splenotropic drug delivery systems. To the best of our knowledge, this is the first report demonstrating impact of nanoparticle shape on *in vivo* performance of nanoparticles.

Splenotropic drug delivery systems designed to enhance splenic uptake, have immense clinical significance for intracellular infections including leishmaniasis, trypanosome, splenic TB, AIDS, malaria, and hematological disorders such as hairy-cell leukemia, idiopathic thrombocytopenic purpura, and autoimmune hemolytic anemia.[1,13–15] The spleen receives barely 15% of an injected dose following intravenous injection of nanocarriers due to rapid clearance from the blood stream by the MPS. Splenotropy therefore demands engineering of "macrophage evading" particulate carriers that upon intravenous injection avoid clearance by hepatic kupffer cells while permitting access and retention in the spleen.[5]

Recently, we have reported polymer lipid nanostructures (LIPOMER) (250–400 nm) of doxycycline hydrochloride (DH) using poly(methylvinylether-co-maleic anhydride) [Gantrez AN119] as polymer and different lipids as matrix material,[16] wherein, in the rat model irregular-shaped glycerylmonostearate (GMS) LIPOMER has shown high splenic uptake

Additional Supporting Information may be found in the online version of this article.

Correspondence to: Prof. Padma V. Devarajan (Telephone: 912224145616; Fax: 912224145614; E-mail: pvdevarajan@gmail.com)

Journal of Pharmaceutical Sciences, Vol. 99, 2576–2581 (2010)

(spleen/liver ratio ~2) while the other LIPOMERs were rapidly cleared by the liver. Moreover, despite similarity in composition, spherical GMS LIPOMER revealed low spleen/liver ratio of <1. Further, both irregularity in shape and spleen/liver ratio increased with increase in GMS concentration. Hence, the objective of the present investigation is to explain this serendipitious finding, namely the role of particle shape in splenotropy.

To rule out the role of GMS in splenotropy solid lipid nanoparticles (SLN) of GMS were prepared and *in vivo* biodistribution evaluated in the rat model. Briefly, 100 mg of each GMS and DH were dissolved in 10 mL of tetrahydrofuran (THF) and added drop-wise to 30 mL aqueous phase containing 25% (w/v) sodium chloride and 1% (v/v) Tween-80 as a surfactant under magnetic stirring. Following complete removal of the solvent, nanosuspensions of the SLN were centrifuged at 15,000 rpm for 30 min at 25°C. Aliquot (0.1 mL) of the supernatant was withdrawn, diluted to 10 mL with distilled water and absorbance recorded at 275 nm using UV spectrophotometer (Shimadzu, Kyoto, Japan). Drug concentration was calculated from standard curve (linearity range 5–30 μg/mL) and entrapment efficiency calculated. Entrapment efficiency of DH was found to be 70.1 ± 0.88% (mean ± SD; $n = 3$). The pellet obtained after centrifugation was suspended in double distilled water. Samples were diluted with double filtered water to obtain appropriate intensity of scattered light and particle size determined by photon correlation spectroscopy using Coulter N4 plus submicron particle size analyzer (Beckman Coulter, CA) by scattering light at 90° at 25°C. The average particle size was found to be 360.6 ± 1.72 nm (mean ± SD; $n = 3$).

Biodistribution of DH solution and DH SLN was carried out in Wistar rats ($n = 4$) as reported earlier for the LIPOMER.[16] Briefly, after radiolabeling with ^{99m}Tc, DH (0.020 mM/kg) or SLN (equivalent to 0.020 mM/kg of DH) were injected through tail vein of the rat. Images were recorded each hour for 5 h under Millennium MPS Acquisition System, (Multipurpose Single Head Square Detector) with a Gamma Camera fitted with Low Energy General Purpose (LEGP) collimator manufactured by G.E. (General Electric, Bucking Hamshire, UK). At the end of 5 h rats were sacrificed and the organs including heart, liver, spleen, kidney, stomach, and intestine were isolated and washed three times with normal saline. Organ associated activity was determined using the gamma camera and % injected dose/g of organ was calculated. All experiments were approved by the Animal Welfare Committee of Bombay Veterinary College. Comparative organ distribution of DH solution and SLN after 5 h of intravenous injection in rats is shown in Figure 1. DH solution mainly

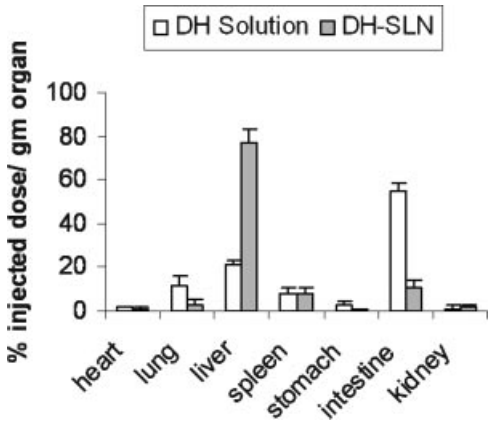

Figure 1. Comparative biodistribution profile of DH solution and DH solid lipidnanoparticles in rats.

concentrated in the intestine. Approximately 75% of the injected dose of SLN of GMS accumulated in the liver, resulting in a low spleen/liver ratio of 0.10 ± 0.04 (mean ± SD; $n = 4$). Scintigraphic images of biodistribution of SLN on rats clearly revealed high liver uptake of SLN (Fig. 2). This ruled out the possibility of GMS as a splenotropic agent.

LIPOMERs of GMS, glyceryltristearate, glycerylpalmitostearate, and stearic acid were prepared as reported earlier.[16] Average particle size of LIPOMERs was in the range of 325–450 nm (Tab. 1). The LIPOMERs and the SLN were evaluated by transmission electron microscopy (TEM; FEI, Eindohoven, the Netherlands) and scanning electron microscopy (SEM; JEOL 840, Tokyo, Japan, magnification: 25,000×; accelerating voltage: 20.0 kV). Briefly, samples were analyzed in the form of aqueous dispersion at 25 ± 2°C.

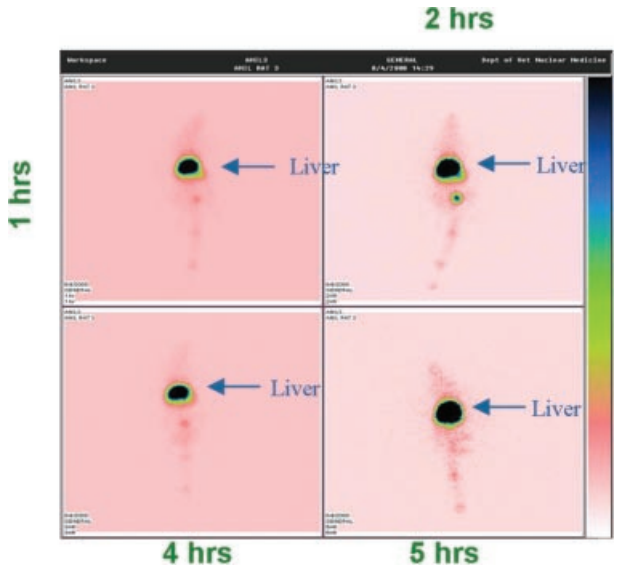

Figure 2. Gamma scintigraphic images of solid lipid nanoparticles in rat at different time intervals.

Table 1. Particle Size and Polydispersity Index (PDI) of Nanoparticles

Sample	Particle Size (Mean ± SD) ($n = 3$)	PDI (Mean ± SD) ($n = 3$)
LIPOMER of glycerylmonostearate	404.60 ± 5.40	0.125 ± 0.98
LIPOMER of glyceryltristearate	361.70 ± 3.40	0.426 ± 1.25
LIPOMER of stearic acid	444.65 ± 5.45	0.219 ± 2.68
LIPOMER of glycerylpalmitostearate	329.25 ± 3.95	0.329 ± 1.96
Solid lipid nanoparticles of glycerylmonostearate	360.6 ± 1.72	0.336 ± 0.69

SEM/TEM images of GMS LIPOMER confirm irregular shape while the LIPOMER of glyceryltristearate, glycerylpalmitostearate, stearic acid and SLN of GMS were spherical/regular in shape (Figs. 3 and 4). Particle size of LIPOMER and SLN is suitable for rapid phagocytic uptake. The high spleen/liver ratio (1.95 ± 0.98, mean ± SD; $n = 4$) of GMS LIPOMER in rat model[16] confirmed the role of particle shape in splenotropy.

Anatomical diversity of mammalian spleen is well established. On the basis of anatomy, spleens characterized as sinusoidal and nonsinusoidal, are also known to exhibit physiological differences.[5] Hence, to understand the mechanism of splenic localization, biodistribution studies were carried out in animal species representing nonsinusoidal spleen (mice) and sinusoidal spleen (rabbit and dog). Swiss albino mice, 4–6 weeks old, weighing 25–30 g ($n = 4$) were housed under standard conditions, had free access to water and were fed standard laboratory chow. Animals were anesthetized by injecting ketamine hydrochloride (0.182 mM/kg) and xylazine hydrochloride (0.038 mM/kg) cocktail intramuscularly 20 min prior to the study. Biodistribution studies were carried out as described for the SLN.

New Zealand rabbits, 6 months to 1 year of age, weighing between 1.5 and 3 kg ($n = 6$) and Labrador dogs ~4 years of age, weighing between 26 and 40 kg ($n = 4$) were selected for the scintigraphic study. As a control, spherical GMS LIPOMER was also evaluated for biodistribution in dogs. Radiolabeled GMS LIPOMER was injected intravenously through the marginal vein of the ear of rabbit and cephalic vein of the dog positioned at 180° under a gamma camera, to acquire scintigraphic images. Images were acquired at 2 h in 256 × 256 matrixes after setting energy level at 140 keV at 20% window for 1 min. The regions of the organs of interest (ROI) were plotted. The data acquired by GENNIE acquisition station was processed on eNTEGRA workstation using the comparative ROI analysis programme.

Biodistribution studies revealed high concentration of GMS LIPOMER in the liver in mice while, in rabbit and dog high concentration was seen in spleen. The spherical GMS LIPOMER on the other hand revealed low splenic concentration and significantly high liver concentration in dog (Fig. 5). The spleen/liver ratio of GMS LIPOMER in different animal species is tabulated in Table 2. The data in Table 2 suggests splenotropic behaviour of irregular GMS LIPOMER in sinusoidal spleen models. Scintigraphic images of the biodistribution of GMS LIPOMER in rabbit and dog are shown in Figures 6 and 7. The images clearly revealed high splenic concentration with the irregular GMS LIPOMER while the spherical GMS LIPOMER accumulated in the liver. Videos showing splenic uptake of the irregular and spherical GMS LIPOMER in dogs are available in supporting information.

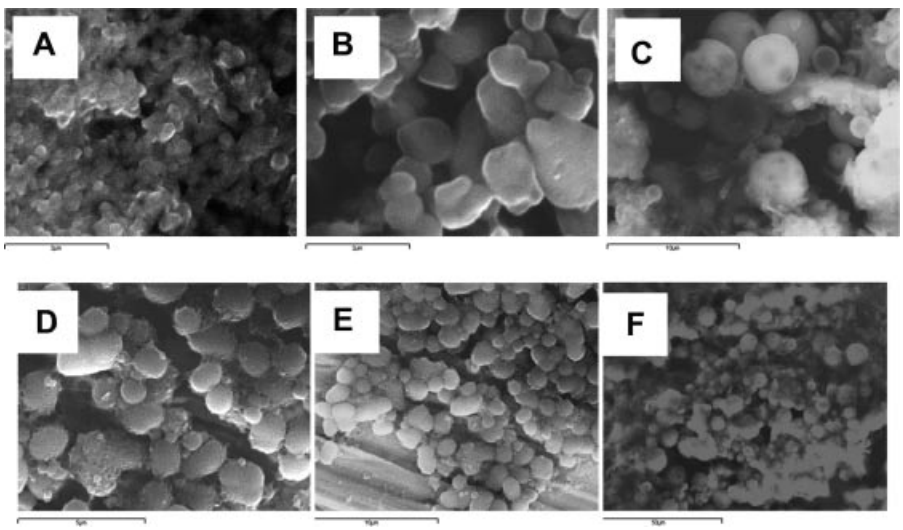

Figure 3. SEM images of (A) spherical GMS LIPOMER, (B) irregular GMS LIPOMER, (C) stearic acid LIPOMER, (D) glyceryl palmitostearate LIPOMER, (E) glyceryltristearate LIPOMER, and (F) solid lipid nanoparticles.

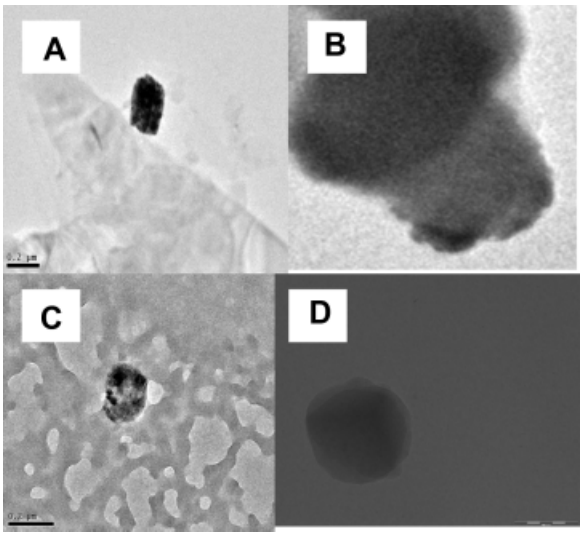

Figure 4. TEM images of LIPOMER of (A) glyceryltristearate, (B) stearic acid, (C) glyceryl palmitostearate, and (D) solid lipid nanoparticles.

Mice spleen which are nonsinusoidal, are characterized by flat endothelial cells and conventional basement membrane and circulating blood passes through large mural apertures. The rabbit, dog, and rat spleen, like human spleen are anatomically characterized as sinusoidal spleens which have longitudinally arranged endothelial cells and a fenestrated basement membrane. Circulating blood passes through the slits between the endothelial cells for draining in to different parts of the spleen. While micron sized red blood cells routinely pass through the spleen, deformed RBCs are trapped and filtered by the spleen.[5] Deformity could therefore induce splenic clearance. The enhanced splenic uptake of cholesterol rich liposomes (50 mol% cholesterol; <200 nm) is reported.[17] However, the reason for their splenotropic behavior is not discussed. Cholesterol is known to decrease the fluidity of liposomes and increases their rigidity. Rigidity of the cholesterol rich liposomes could have played an important role in

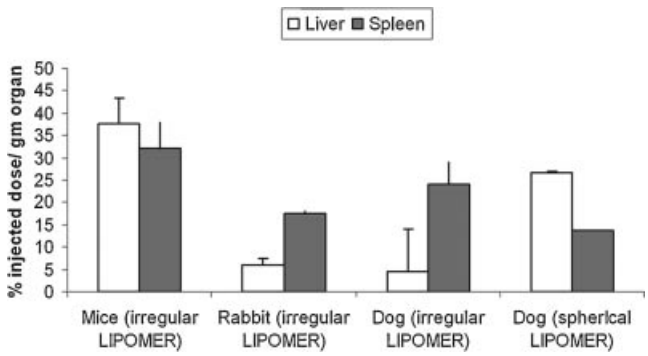

Figure 5. Biodistribution profile of GMS LIPOMER in different animal models.

Table 2. Spleen/Liver Ratio of GMS LIPOMER in Different Animal Models

Animal Models	GMS LIPOMER	Spleen Anatomy	Spleen/Liver Ratio (Mean ± SD) ($n = 4$)
Mice	Irregular	Nonsinusoidal	0.91 ± 0.36
Rabbit	Irregular	Sinusoidal	2.86 ± 1.31
Dog	Irregular	Sinusoidal	6.77 ± 1.79
Dog	Spherical	Sinusoidal	0.53 ± 0.15

their splenic clearance. Based on the above, we attribute the splenotropic behavior of irregular GMS LIPOMER to a combination of rigidity and deformity of nanoparticles. It is probable that the irregular-shaped GMS LIPOMER was recognized as a deformed particle by the splenic vasculature.

An important strategy for splenotropy is the design of macrophage-evading carriers which bypass hepatic clearance but accumulate in the spleen. To confirm the macrophage-evading characteristic, *in vitro* phagocytic uptake of fluorescent-labeled spherical and irregular GMS LIPOMER was studied following a previous method with some modifications.[18] Fluorescent-labeled GMS LIPOMER was prepared by modification of the method reported earlier.[16] Coumarin (1 mg) was dissolved in the organic phase with DH prior to nanoparticle preparation using water or water–isopropyl alcohol (1:1) as the nonaqueous phase to obtain the spherical and irregular LIPOMER, respectively. A moist chamber was prepared by placing wet cotton in a Petridish. Blood (3–4 drops) was collected on a clean glass slide, placed in the moist chamber and incubated at 37°C for 25 min. The clot on the slide was teased off gently and separated from the white blood cells (WBC) using a needle and

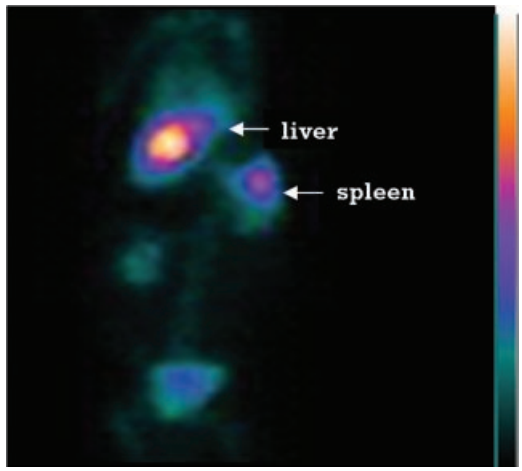

Figure 6. Gamma scintigraphic image of biodistribution of irregular GMS LIPOMER in rabbit.

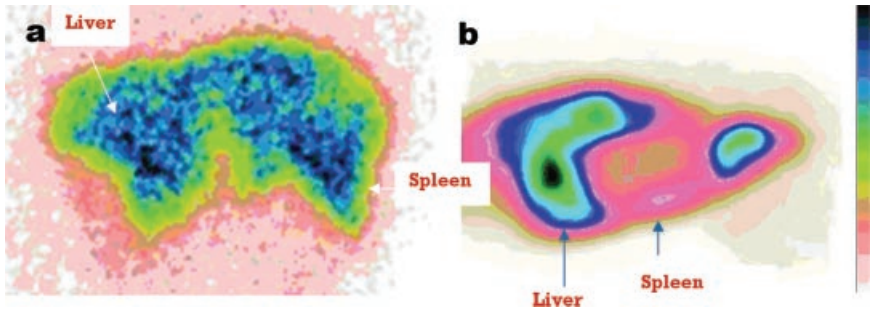

Figure 7. Gamma scintigraphic images biodistribution of GMS LIPOMER in dog (a) irregular, (b) spherical.

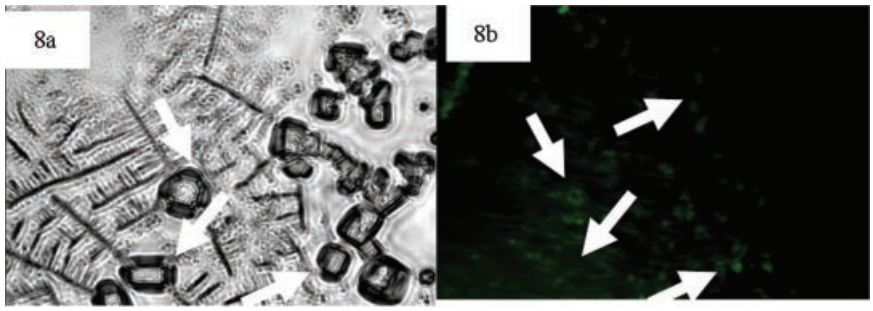

Figure 8. *In vitro* uptake of irregular GMS LIPOMER by white blood cells (a) optical mode (arrows indicate WBC) (b) fluorescent mode (arrows indicate location of WBC).

the residual WBC enriched blood washed with normal saline carefully. After removal of the clot, WBC's were flooded with 50 μL of LIPOMER dispersion equivalent to 35 μg of DH, incubated at 37°C for 5 min and washed with 0.9% (w/v) sodium chloride solution. Subsequently, the slide was stained with Leishman's stain for 15 min and observed under a fluorescent microscope (Olympus, Hamburg, Germany). Images were acquired under optical and fluorescence mode for the same slide area.

The data on *in vitro* phagocytic uptake studies is depicted in Figures 8 and 9. WBC are marked by arrows in Figures 8a and 9a, representing the optical mode, while the arrows in Figures 8b and 9b point out the location of the WBC (not seen) in the fluorescence mode. Appreciable fluorescence (Fig. 9b) as opposed to marginal fluorescence (Fig. 8b) reveals high uptake of the spherical GMS LIPOMER and poor uptake of the irregular GMS LIPOMER, thereby confirming the macrophage-evading characteristic of the irregular GMS LIPOMER. The report by Mitragotri and Champion,[11,12] wherein they demonstrated that irregular-shaped particles bypassed phagocytosis due to incomplete actin structure formation, further supports our finding of the role of nanoparticle shape on bypass of phagocytic uptake.

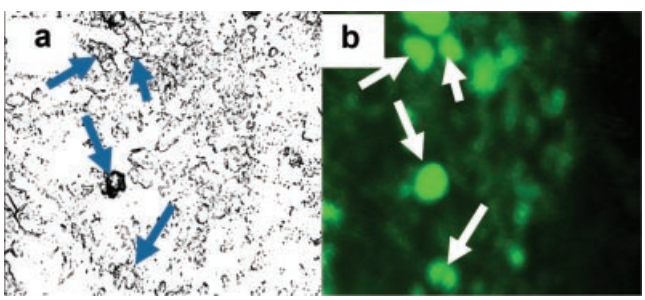

Figure 9. *In vitro* uptake of spherical GMS LIPOMER by white blood cells (a) optical mode (arrows indicate WBC) (b) fluorescent mode (arrows indicate location of WBC).

Our study suggests that irregular GMS LIPOMER on intravenous administration evades macrophages to reach the spleen in high concentration. In the sinusoidal spleen the LIPOMER recognized as a deformed structure is cleared and accumulates to exhibit splenotropy.

The exciting conclusion of this investigation is the finding that particle shape could prove an important tool in the design of splenotropic drug delivery systems. This study provides the first proof of concept of the role of particle shape on *in vivo* performance of the nanocarrier systems. Particle shape as a parameter could open up exciting possibilities as a novel approach in passive targeting. Nevertheless, two aspects that need further investigation include the role of opsonins on the biodistribution behavior of

irregular GMS LIPOMER and the physics of formation of the irregular-shaped particles.

ACKNOWLEDGMENTS

Anil B. Jindal is thankful to University Grant Commission, Government of India, for fellowship. Authors are thankful to Dr. Sadhana Sathaye, Institute of Chemical Technology, Mumbai and Dr. Amit Misra, Central Drug Research Institute, Lucknow for valuable discussions, Dr. Pushan Ayub, Tata Institute of Fundamental Research, Mumbai for SEM and TEM studies, Anshul Agencies India and ISP, Inc. for sample of Gantrez and Gattefosse SA, France for the lipid samples.

REFERENCES

1. Moghimi SM, Hunter AC, Murray JC. 2001. Long-circulating and target-specific nanoparticles: Theory to practice. Pharmacol Rev 53:283–318.
2. Moghimi SM. 1995. Exploiting bone marrow microvascular structure for drug delivery and future therapies. Adv Drug Deliv Rev 17:61–73.
3. Banerjee T, Mitra S, Kumar SA, Kumar SR, Maitra A. 2002. Preparation, characterization and biodistribution of ultrafine chitosan nanoparticles. Int J Pharm 243:93–105.
4. Storm G, Belliot SO, Daemen T, Lasic DD. 1995. Surface modification of nanoparticles to oppose uptake by the mononuclear phagocyte system. Adv Drug Deliv Rev 17:31–48.
5. Moghimi SM. 1995. Mechanisms of splenic clearance of blood cells and particles: Towards development of new splenotropic agents. Adv Drug Deliv Rev 17:103–115.
6. Allen TM. 1994. The use of glycolipids and hydrophilic polymers in avoiding rapid uptake of liposomes by the mononuclear phagocyte system. Adv Drug Deliv Rev 13:285–309.
7. Patil RR, Guhagarkar SA, Devarajan PV. 2008. Engineered nanocarriers of doxorubicin: A current update. Crit Rev Ther Drug Carrier Syst 25:1–61.
8. Moghimi SM, Porter CJH, Muir IS, Illum L, Davis SS. 1991. Nonphagocytic uptake of intravenously injected microspheres in rat spleen: Influence of particle size and hydrophilic coating. Biochem Biophys Res Commun 991:861–866.
9. Moghimi SM, Hedeman H, Muir IS, Illum L, Davis SS. 1993. An investigation of the filtration and the fate of large filtered sterically-stabilized microspheres in rat spleen. Biochim Biophys Acta 1157:233.
10. Peracchia MT, Attal EF, Desmaele D, Besnard M, Noel JP, Gomis JM, Appel M, Couvreur PJ. 1999. Stealth PEGylated polycyanoacrylate nanoparticles for intravenous administration and splenic targeting. J Control Release 60:121–128.
11. Champion JA, Mitragotri S. 2006. Role of target geometry in phagocytosis. Proc Natl Acad Sci USA 103:4930–4934.
12. Champion JA, Mitragotri S. 2009. Shape induced inhibition of phagocytosis of polymer particles. Pharm Res 26:244–249.
13. Melo RC, Brener Z. 1978. Tissue tropism of different Trypanosoma cruzi strains. J Parasitol 64:475–482.
14. Joshi S, Bankar M, Kagal A, Rane S, Bharadwaj R, Phadke M. 2007. Splenic tuberculosis—A rare case report. Internet J Med Update 2:21–25.
15. Gratton S, Cheynier R, Dumaurie M, Oksenhendle E, Hobson SW. 2000. Highly restricted spread of HIV-1 and multiply infected cells within splenic germinal centers. Proc Natl Acad Sci USA 97:14566–14571.
16. Patil RR, Gaikwad RV, Samad A, Devarajan PV. 2008. Role of lipids in enhancing splenic uptake of polymer-lipid (LIPOMER) nanoparticles. J Biomed Nanotech 4:359–366.
17. Moghimi SM, Patel HM. 1988. Tissue specific opsonins for phagocytic cells and their affinity for cholesterol rich liposomes. FEBS Lett 233:143–147.
18. Wadekar RR, Agrawal SV, Tewa KM, Shinde RD, Mate S, Patil K. 2008. Effect of Baliospermum montanum root evtract on phagocytosis by human neutrophils. Int J Green Pharm 2: 46–49.